

Attenuation process of the longitudinal phonon mode in a TeO₂ crystal in the 20-GHz rangeS. Ohno,^{1,*} T. Sonehara,¹ E. Tatsu,¹ A. Koreeda,² and S. Saikan¹¹*Department of Physics, Graduate School of Science, Tohoku University, Sendai, 980-8578, Japan*²*Department of Physical Sciences, College of Science and Engineering, Ritsumeikan University, Kusatsu 525-8577, Japan*

(Received 13 July 2016; revised manuscript received 15 May 2017; published 5 June 2017)

We experimentally investigated the hypersonic attenuation process of a longitudinal mode (L-mode) sound wave in TeO₂ from room temperature to a lower temperature using Brillouin scattering and impulsive stimulated thermal scattering (ISTS) measurements. For precise measurement of the Brillouin linewidth at low temperatures, whereby the mean free path of the phonon becomes longer than the sample length, it is indispensable that the phonon should propagate along the phonon-resonance direction. To figure out the suitable direction, we defined two indices characterizing a degree of phonon divergence and a purity of propagation direction. The best direction that we found from these indices is [110] direction in TeO₂, and it was used to discuss the temperature and frequency dependences of Brillouin spectra. We extracted the temperature dependence of the attenuation rate of T^4 from the modulated Brillouin spectra due to the phonon resonance below Debye temperature. The frequency dependence ω^1 of the hypersonic attenuation was also estimated from the polarization dependence of the Brillouin linewidth. Theoretically, it predicted that the L-mode phonon attenuation at low temperatures in TeO₂ is a result of Herring's process, which shows the attenuation behavior of $\omega^2 T^3$. The $\omega^1 T^4$ dependence is not allowed in Herring's process but is allowed by the $L + L \rightarrow L$ process, which has been considered to be forbidden so far. We evaluated the thermal phonon lifetime using ISTS and established that it was finite even at 20 K, thereby allowing the $L + L \rightarrow L$ process. Therefore, we conclude that the $L + L \rightarrow L$ process dominates the attenuation of an L-mode phonon in TeO₂ in the low-temperature region.

DOI: [10.1103/PhysRevB.95.224301](https://doi.org/10.1103/PhysRevB.95.224301)**I. INTRODUCTION**

Phonon-scattering processes in crystals is a long-standing subject in the fundamental physics of condensed matter [1,2], moreover it is also an attractive issue from engineering that treats recent thermal transfer problems [3,4]. Recent improvements in techniques of radio frequency and lasers have enabled very precise measurements of high-frequency acoustic phonons.

We have developed a high-resolution, high-sensitivity stimulated Brillouin spectrometer [5,6], and it has been applied to investigate the elastic properties of some materials at low temperatures [7–11]. In crystals, the stimulated Brillouin spectrum at low temperatures can be substantially modulated (“jagged”) as we reported in Ref. [5], due to the multiple reflection of long-lived phonons at the sample boundaries. Although the effect had obscured precise estimate of the phonon lifetime, our recently-established methodology [12] has enabled us to successfully extract the essential lifetime of the longitudinal (L)-mode phonons in a TeO₂ crystal, even from a modulated Brillouin spectrum.

The hypersonic attenuation in TeO₂ was reported by Damen *et al.*, and their experimental results were accounted for in terms of the phonon-phonon scattering process [13]. They argued that Herring's scattering process [14], in which an L-mode phonon collides with a slow transverse mode phonon (ST-mode) and then a fast transverse mode (FT-mode) phonon is created, $L + ST \rightarrow FT$, was observed in the phonon propagating along the [001] direction. However, Tamura *et al.* theoretically showed [15] that the Herring's process along the [001] direction cannot occur and they concluded that Herring's

process could not account for the experimental results of Damen *et al.* when the thermal phonon lifetime was not taken into account. The purpose of the present paper is to clarify the attenuation process of an L-mode phonon in TeO₂ by considering the thermal-phonon lifetime measured in the low-temperature range as well as the appropriate treatment of the modulated Brillouin spectra.

Historically, the discussions taking account of a finite lifetime of thermal phonon at the temperature region in which the sound wave duration $1/\omega$ is shorter than the thermal phonon lifetime τ , i.e., $\omega\tau > 1$, have been succeeded to explain the attenuation behavior in various materials. A finite lifetime of thermal phonon changes the situation of the selection rule derived on three phonon processes assuming the infinite thermal phonon lifetime. Experimental [16,17] and theoretical [18] works in quartz crystal have been revealed that the $L + L \rightarrow L$ process can be allowed by considering the finite τ . Furthermore strong temperature dependence of the attenuation rate shown in the low temperature region in quartz crystal has been turned out to be attributed to the temperature dependence of τ . In silicon, a finite thermal phonon lifetime has been required to explain the attenuation process of L and T mode waves [19]. Recently, subterahertz acoustic phonon attenuation due to Herring process has been reported in composite semiconductors, e.g., GaN [20], GaAs [21], with ground swell of interest in thermoelectric and/or nanodevices. These experimental conditions were designed so that $\omega\tau$ was much larger than unity. We consider that the finite lifetime of thermal phonon should be taken into account in TeO₂ as well. In the present work, we experimentally estimate the value $\omega\tau$ in TeO₂ and discuss the origin of the L-mode phonon attenuation based on the value.

TeO₂ has been utilized in acousto-optic devices due to its highly photoelastic performance. To reveal the attenuation

*seigo@m.tohoku.ac.jp

process in TeO_2 is important not only from the viewpoint of fundamental material physics but also from the engineering for photoelastic devices including phononic metamaterials. As it has been discussed in photonic metamaterials [22,23], the attenuation of wave is one of the significant features to characterize the functionalities of a consisting metamaterial. We consider that the investigation of attenuation process in functional materials is one of conventional and novel issues.

In the next section, we introduce two indices to assess and quantify the phonon divergence and the purity of propagation in order to determine the best direction for the phonon resonance. Then we briefly review some theoretical predictions that have been reported so far in regard to the behaviors of the hypersonic attenuation depending on temperature and phonon frequency. In the experimental section, we show the analyzed results of the Brillouin spectra and thermal phonon lifetimes obtained by impulsive stimulated thermal scattering measurement (ISTS) in a TeO_2 crystal. After that, we discuss the origin of the behavior of the attenuation rate and finally show our conclusions.

II. THEORETICAL BACKGROUND

In this section we introduce and organize some theoretical background necessary for discussion of the attenuation process of phonons in a crystal.

A. Optimal direction for Brillouin spectroscopy

The phononic properties of a crystal are characterized by the crystal's anisotropic features [1,24–26], which affects the propagation direction of sound waves. We have to treat the anisotropy carefully in the Brillouin scattering measurement at low temperature, in which the mean free path of a phonon is longer than the size of the interaction region characterized by the laser beam width and the sample length. As we pointed out in Ref. [12], one must confine the phonon in the interaction region in a crystal and cause the phonon to undergo multireflection along the pure propagation direction. In practice, this lengthens the interaction length enough to estimate the attenuation rate from the Brillouin spectra.

At low temperature, phonon divergence and off-axis propagation make the interaction length shorten. In order to estimate the two kinds of propagation properties, we propose corresponding indices of $\mathbf{div} \mathbf{v}_g''$ and β . $\mathbf{div} \mathbf{v}_g''$ shows the degree of divergence of a phonon through the propagation. Since a large value means that the phonon beam is apt to diverge while propagating, one should choose the minimum value direction for the phonon propagation as to avoid phonon divergence effect. This index is very similar to the inverse of phonon focusing factor introduced by Maris [27,28] whereas a factor of inner product with a phonon wave vector \mathbf{q} does not appear in our index. In order to separate the purity of propagation of phonons from the phonon divergence (focusing) effect, the angle between the energy flux and the wave vector, β , is appropriate as another index: a direction of $\beta = 0$ is called the pure propagation direction. The definition and the derivation of these indices are detailed in Appendix A. By using these indices, one can find a suitable direction to measure phonon attenuation rate through the multireflection of phonon.

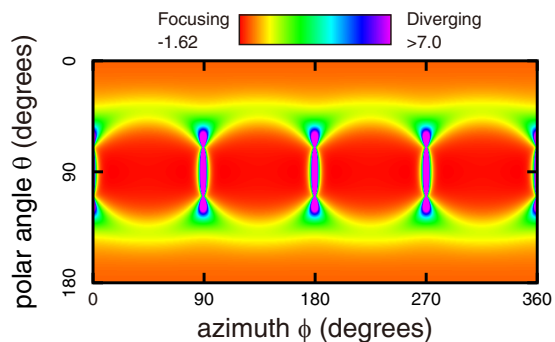


FIG. 1. Distribution of $\mathbf{div} \mathbf{v}_g''$ for the L-mode phonon in TeO_2 crystal.

The distribution of $\mathbf{div} \mathbf{v}_g''$ for an L-mode phonon on the (θ, ϕ) plane of a TeO_2 crystal is shown in Fig. 1. In this calculation, we used the values of density and the stiffness tensor given in Ref. [29]. In the figure, the red and purple regions indicate the focusing and diverging directions, respectively. It can be seen that the directions of the minimal index were $[110]$ $[(\theta, \phi) = (90^\circ, 45^\circ)]$ and $[001]$ $(\theta = 0^\circ)$, as well as their symmetrical equivalents. Hence, the divergence of phonons propagating in these directions is suppressed. In particular, since the red region around the $[110]$ direction is quite wide, this direction has an advantage in robustness against experimental misalignment of the laser beam. On the contrary, in the $[100]$ $[(\theta, \phi) = (90^\circ, 0^\circ)]$ direction, the phonon is likely to diverge.

In an L-mode phonon in TeO_2 crystal, the distribution of β is shown in Fig. 2. In this figure, the region $\beta < 5^\circ$ is colored in order to emphasize the tiny variation of the index of purity. We find that the directions $[100]$, $[001]$, and $[110]$, as well as the direction around $(\theta = 40^\circ, \phi = 45^\circ)$ and their symmetrical equivalents, are pure propagation directions.

From the results of the indices both for the divergence and for the purity of the propagating L-mode phonon in TeO_2 , the phonon along the $[110]$ direction is found to propagate with the lowest divergence and perfect purity. Thus, we can conclude that the $[110]$ direction is the most appropriate for measuring the Brillouin spectrum in TeO_2 at low temperature.

B. Supersonic attenuation process

In this section, we summarize the theories to date for the supersonic attenuation process of the L-mode phonon in

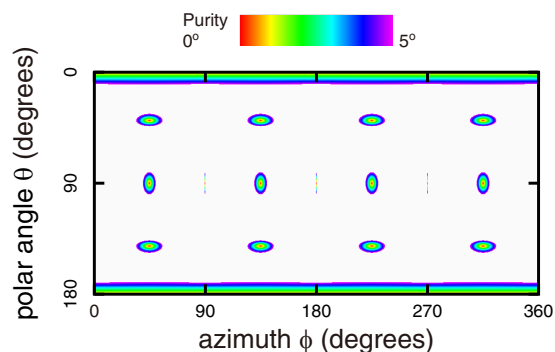


FIG. 2. The index of pure propagation in an L-mode phonon of TeO_2 crystal.

TABLE I. Scattering process, coefficient a, b in $\Gamma_{\Lambda_1} \propto \omega_{\Lambda_1}^a T^b$, and assumed condition of thermal phonon lifetime τ .

| Process | Dependence | | Lifetime τ | Remarks | Reference |
|-------------------------|------------|-----|-----------------|---|-----------|
| | a | b | | | |
| $L + L \rightarrow L$ | 1 | 4 | ∞ | Collinearly ordered in a Herring diagram | [26] |
| | 1 | 4 | finite | Allowed due to uncertainty of thermal phonon energy | [18,26] |
| | 0 | >6 | finite | Temperature dependence of τ is predominant. | [17,26] |
| $L + FT \rightarrow FT$ | 1 | 4 | finite | Forbidden when $\tau \rightarrow \infty$ due to mode dispersion | [17,26] |
| $L + T \rightarrow L$ | 4 | 1 | ∞ | | [25] |
| $L + ST \rightarrow FT$ | 2 | 3 | ∞ | Herring process is forbidden in isotropic materials | [14,15] |

crystals. In particular, we briefly review three-phonon process and Akhiezer damping, which are dominant at low temperature and room temperature, respectively.

1. Three phonon process

In the 1950s, Landau and Rumer considered that collision with a thermal phonon, termed the three-phonon process, may cause supersonic attenuation in crystals [30]. In their discussion, the anisotropy of the crystal was neglected and the thermal phonon lifetime τ was not considered, namely τ was assumed to be infinite. Later, the theory of the three-phonon process was improved to consider the dispersion of the sound velocity. According to the theory [15,26], the phonon under consideration, Λ_1 , collides with a thermal phonon, Λ_2 , and generates another thermal phonon, Λ_3 ; the attenuation rate Γ_{Λ_1} can be written as

$$\Gamma_{\Lambda_1} = \frac{\pi \hbar}{8\rho^3 V \omega_{\Lambda_1}} \sum_{\Lambda_2, \Lambda_3} \frac{|\Phi_{\Lambda_1 \Lambda_2 \Lambda_3}|^2}{\omega_{\Lambda_2} \omega_{\Lambda_3}} 2(n_{\Lambda_2}^0 - n_{\Lambda_3}^0) \times \delta(\mathbf{q}_{\Lambda_1} + \mathbf{q}_{\Lambda_2} - \mathbf{q}_{\Lambda_3}) \delta(\omega_{\Lambda_1} + \omega_{\Lambda_2} - \omega_{\Lambda_3}), \quad (1)$$

where $\Phi_{\Lambda_1 \Lambda_2 \Lambda_3}$ is a three-phonon matrix element including information about the stiffness tensor and the anharmonicity tensor in a crystal and $n_{\Lambda_i}^0$ denotes the Bose-Einstein (BE) distribution function for the phonon Λ_i . The BE distribution function depends upon the temperature of the crystal. The energy of the phonons under consideration is conserved by the term $\delta(\omega_{\Lambda_1} + \omega_{\Lambda_2} - \omega_{\Lambda_3})$, which originates with Fermi's golden rule. The derivation of the delta function is based on the assumption that the lifetime of the thermal phonons is sufficiently longer than the interacting time. In view of this premise, the theory of the three-phonon process is mainly applicable at lower temperature than the Debye temperature of the crystal. The term $\delta(\mathbf{q}_{\Lambda_1} + \mathbf{q}_{\Lambda_2} - \mathbf{q}_{\Lambda_3})$ is related to momentum conservation. The summation $\sum_{\Lambda_2, \Lambda_3}$ running over all thermal phonon modes that satisfy both energy and momentum conservation contributes to the attenuation rate in the three-phonon process in a crystal at low temperature. Hereafter, we will omit the subscription beside the phonon mode for simplicity according to the conventional notation, e.g., $L + L \rightarrow L$, in which the terms indicate Λ_1 , Λ_2 , and Λ_3 from the left, respectively.

The contribution to the attenuation rate was classified into some kinds of scattering processes according to different vibration modes of the thermal phonon and the way how the models deal with their lifetimes. In Table I, we can see the classified processes that have been predicted in the literature,

together with their temperature and frequency dependences [14,15,17,18,25,26]. For the cases of the infinite thermal phonon lifetime in the table, one can see the relation

$$\Gamma_{\Lambda_1} \propto \omega_{\Lambda_1}^a T^b \quad a + b = 5, \quad (2)$$

which is known as Herring's scaling rule [14]. This relation is useful to indicate validity for both frequency and temperature dependences of attenuation rate given by the analysis of experimental results.

In particular, the $L + L \rightarrow L$ process under the condition of infinite thermal phonon lifetime can be satisfied only in the situation where all the wave vectors of the three phonons are similarly directed, since the wave vectors of the L-mode phonon are shorter than those of two other T modes. Herring's diagram for the $L + L \rightarrow L$ process along the [110] direction in TeO₂ is shown in Fig. 3 [14]. The slowness

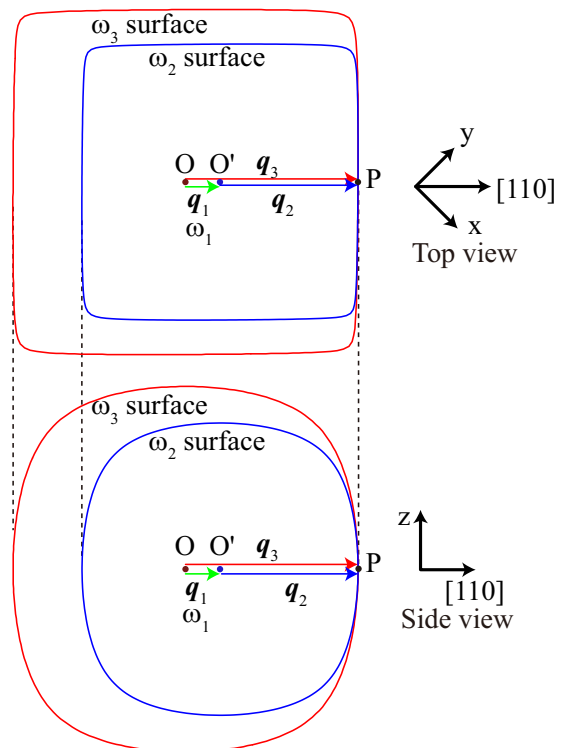


FIG. 3. Herring's diagram for the $L_1 + L_2 \rightarrow L_3$ process in TeO₂ along the [110] direction. Upper and lower panels depict the cross sections of the slowness surfaces within the xy - and z -[110] planes, respectively.

surfaces for ω_2 and ω_3 have origins O and O' , respectively; the displacement between these origins is \mathbf{q}_1 . The slowness surfaces touch together at point P . The vectors \overrightarrow{OP} and $\overrightarrow{O'P}$, respectively, correspond to \mathbf{q}_3 and \mathbf{q}_2 . Considering an apparent characteristic of a slowness surface of L mode on which has no negative curvatures, a strict energy-conservation rule related to participating phonons, consequently, guides such a situation of a point contact. Furthermore, the momentum conservation in the $L + L \rightarrow L$ process is not possible owing to both the frequency dispersion of the acoustic phonon and the long-wave-vector feature of the thermal phonon. This situation is very similar with the difficulty to satisfy the phase matching condition of nonlinear optical effects in a dispersive nonlinear crystal [31]. Hence, it has been believed that the $L + L \rightarrow L$ process does not dominate attenuation in TeO₂.

However, if finite thermal phonon lifetime is assumed, $L + L \rightarrow L$ can be allowed. For example, the $L + L \rightarrow L$ in a quartz has been observed and b becomes higher than 6, due to temperature dependence of τ [17, 18]. In TeO₂, the fact that the two slowness surfaces, shown in Fig. 3, have approximately the same positive curvature in the vicinity of the point of contact plays an important role in the case that the uncertainty of energy is allowed as discussed later.

2. Akhiezer damping

Akhiezer [32] described the phonon attenuation of sound wave when the lifetime of the thermal phonon τ is significantly shorter than the oscillation period of the considered sound wave $1/\omega$, namely, $\omega\tau \ll 1$, thus it should be realized at room temperature. This theory incorporates the energy loss which is attributed to a modulated thermal equilibrium state of the thermal phonons due to the deformation by the sound wave. Accordingly, the attenuation is given as [26,33]

$$\Gamma = \frac{C_V \gamma^2 T \omega^2 \tau}{3\rho v^3}, \quad (3)$$

where γ is the Grüneisen constant of a crystal. Using the thermal conductivity relation $\kappa = \frac{1}{3}C_V v^2 \tau$, Γ is written as

$$\Gamma = \frac{\gamma^2 \kappa T \omega^2}{3\rho v^5}. \quad (4)$$

This means that the attenuation rate linearly depends on the temperature around this temperature region. Furthermore, since in the case of sufficient high-temperature limit, temperature dependence of κ becomes $\kappa \propto 1/T$, the attenuation rate is independent of the temperature [34].

III. EXPERIMENTS

A. Stimulated Brillouin scattering measurement

1. Temperature dependence

Previously, we measured the temperature dependence of the stimulated Brillouin spectra of the L-mode phonon in TeO₂ crystal with a high resolution stimulated Brillouin spectrometer [5]. The measurement setup is shown in Fig. 4. Tunable monolithic type lasers are employed as pump and probe beam. The frequency difference between the two lasers is real-time monitored through the beat frequency measurement

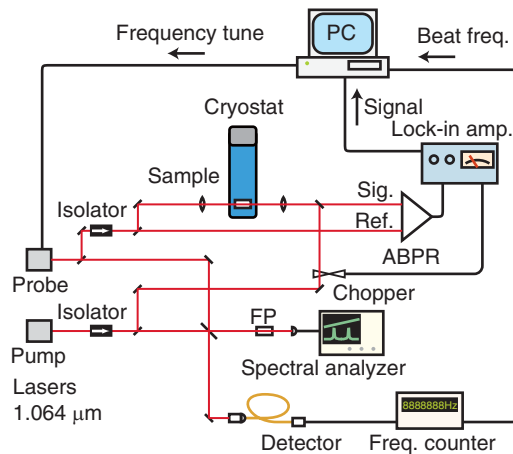


FIG. 4. Experimental setup for a stimulated Brillouin scattering spectrometer. Monolithic type Nd:YAG lasers are used for the pump and probe lasers. The frequency difference between the pump and probe waves is real-time monitored by using a frequency counter through the beat frequency between the waves. The counterpropagating laser beams are focused into a sample crystal in a continuous flow type cryostat. FP and ABPR denote a scanning Fabry-Perot interferometer and an auto-balanced photoreceiver, respectively. See Ref. [12] for details.

by a frequency counter. The use of stable monolithic type lasers and the real-time monitoring of the frequency difference enable us to achieve very high frequency resolution of 20 kHz. The counterpropagating pump and probe beams are focused into a continuous-flow type cryostat in which a TeO₂ crystal was set.

In the measurement, the directions of phonon propagation and the polarization of both the pump and probe laser beams were set to [110] and [001], respectively. The conditions to observe Brillouin signal in an anisotropic crystal are available by using the selection rule of the Brillouin scattering [35]. As the above discussion suggests, [110] in TeO₂ is the best direction for measuring the Brillouin scattering at low temperature using the L-mode phonon, so that we succeeded in observing the spectral modulation at low temperatures by reflecting the phonon resonance effect.

The obtained Brillouin spectra in a 5 mm thickness sample along the [110] direction are shown in Fig. 5 with blue symbols, from which, in our previous work [12], we have selectively introduced characteristic spectra. The Brillouin frequency gradually moves to a high frequency region with decreasing temperature. The linewidth narrows and the spectral shape was significantly modulated from trivial Lorentz function to multippeak structure below 50 K. The modulated spectrum was reproduced by the model in which the phonon resonated in a one-dimensional system. We were also able to estimate the attenuation rate from the modulated spectrum [12]. The analyzed temperature dependence of the attenuation rate is shown in Fig. 6.

In the temperature region from 10 to 50 K, the attenuation agreed with $\Gamma \propto T^4$. Gradually, the slope decreased as the temperature increased and finally became shallower than $\Gamma \propto T^1$ at room temperature. Below 10 K, the attenuation rate could not be measured precisely because it is comparable with

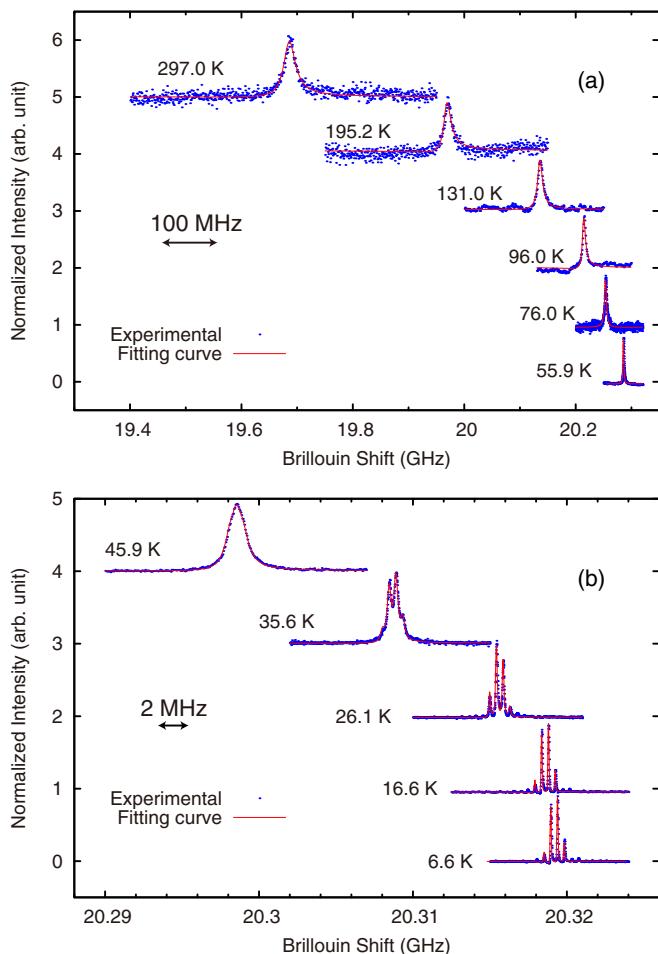


FIG. 5. Temperature dependence of Brillouin spectrum of an L-mode phonon in TeO₂, [110] direction measured above (a) and below (b) 50 K. The spectra are offset vertically for clarity.

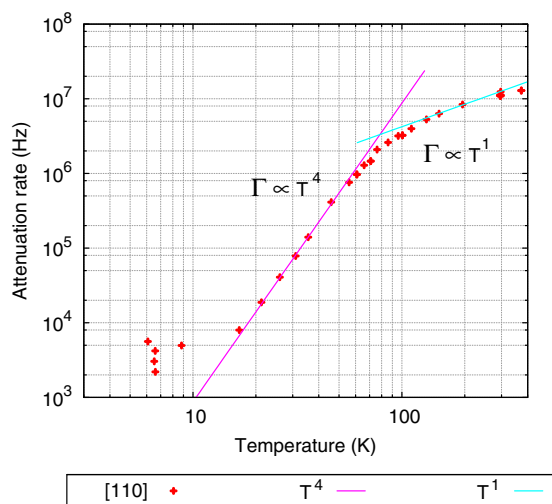


FIG. 6. Temperature dependence of the attenuation rate of an L-mode phonon in TeO₂, [110] direction. The corresponding phonon frequency was around 20 GHz as shown in Fig. 5.

the spectral resolution of 20 kHz of the spectrometer. The behavior of the temperature dependence of the Brillouin shift is not presented here but followed our previous work [7].

2. Frequency dependence

To obtain the frequency dependence of the attenuation rate, one must measure the Brillouin linewidth with changing ω_B . Here, we tried to measure the frequency dependence of the attenuation rate utilizing the high spectral resolution of our Brillouin spectrometer. In the condition of Brillouin scattering, the Brillouin shift ω_B is given by

$$\omega_B = 2\Omega n \frac{v}{c} \sin \frac{\theta}{2}, \quad (5)$$

where Ω is the angular frequency of the incident light, c is the speed of light, n is the refractive index of the medium, and θ is the scattering angle. In general, the spontaneous Brillouin scattering measurements can change ω_B by tilting the incident angle $\theta/2$. However, we had to devise another approach as to utilize the same experimental setup from the following reasons: (i) a back-scattering setup ($\theta = \pi$) for a sufficiently long interaction length to get a high signal-to-noise ratio and to suppress transit time broadening of the Brillouin linewidth, and (ii) a limit of tunable range of laser waves up to $\Delta\Omega/2\pi = 30$ GHz that implies a too small change of $\Delta\omega_B/\omega_B \sim 0.01\%$ to reveal the frequency dependence.

Our idea for changing ω_B was to apply the difference in the refractive indices of ordinary and extraordinary waves, i.e., n_o and n_e , in a uniaxial crystal. According to Ref. [36], the refractive indices in TeO₂ are given as $n_o = 2.2005$, or $n_e = 2.3431$ for a 1.0642 μm light. In this case, $\Delta\omega_B/\omega_B \sim 6\%$ is expected, and it may be possible to detect the frequency dependence of the attenuation rate in the temperature region in which the Brillouin linewidth is relatively broad.

We measured the Brillouin spectrum in the L-mode phonon along the [110] direction of TeO₂ at several temperatures, including 373, 298, 100, and 70 K, with polarization directions of [110] and [001] being the ordinary and extraordinary directions, respectively. A sample was set into a cryostat and an oven for the measurements below and above room temperatures, respectively. The cryostat has a thermometer which enables us to acquire temperature in real time. We could precisely estimate the temperature fluctuation during the data integration. On the other hand, our oven did not have any system to output monitoring temperature.

The most prominent difference in the linewidth was observed at 373 K, as shown in Fig. 7. In this figure the central frequencies of both spectra are shifted for comparison of the linewidth, and the signal height is normalized to unity. The center frequencies of the spectra for ordinary and extraordinary were observed 18.258 96 and 19.437 33 GHz by our high resolution Brillouin scattering spectroscopic system, respectively. It is observed that the spectral linewidth provided by the ordinary index is significantly narrower than the other.

The analyzed results of frequency dependence as a function of temperature are shown in Fig. 8. The frequency dependence a on the vertical axis is obtained by

$$a = \frac{\log(\Gamma(n_e)/\Gamma(n_o))}{\log(\omega_B(n_e)/\omega_B(n_o))}, \quad (6)$$

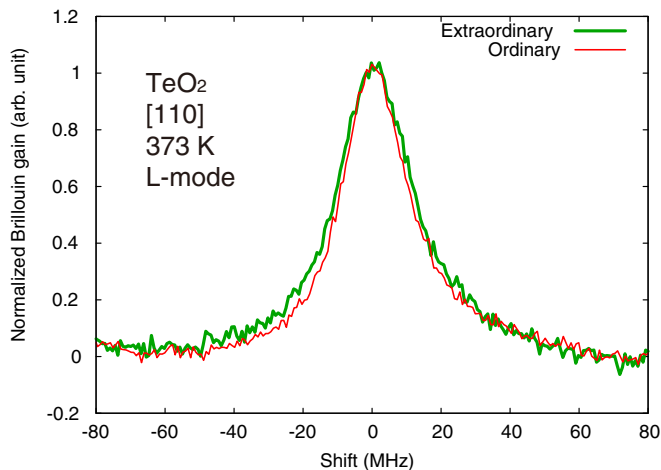


FIG. 7. Comparison of Brillouin spectra obtained in TeO₂, [110] direction, L-mode phonon at 373 K. Green and red curves show the spectra in n_e and n_o , respectively.

where $\Gamma(n)$ and $\omega_B(n)$ are, respectively, the Brillouin linewidth and the shift of the refractive index n . Hence, the relationship between a and Γ is given by

$$\Gamma \propto \omega^a. \quad (7)$$

The temperature dependence of a is shown in Fig. 8. We estimated experimental error bars through the spectral broadening $\Delta\Gamma$ due to the temperature fluctuation ΔT during the measurement as

$$\Gamma + \Delta\Gamma \simeq \Gamma + \frac{\partial\omega_B}{\partial T} \Delta T, \quad (8)$$

where $\partial\omega_B/\partial T$ means Brillouin shift change with temperature. We could estimate the error bars only for the red symbols measured in the cryostat but not for the green crosses measured in the oven. The value of a is around 2 above room temperature and decreases with temperature. Below 100 K, a is sufficiently less than 2 even with taking into account its large error bar.

B. ISTS measurement

In earlier discussions about the attenuation process of an L-mode phonon in TeO₂, it is assumed that the lifetime of the thermal phonon is much longer than the interaction time

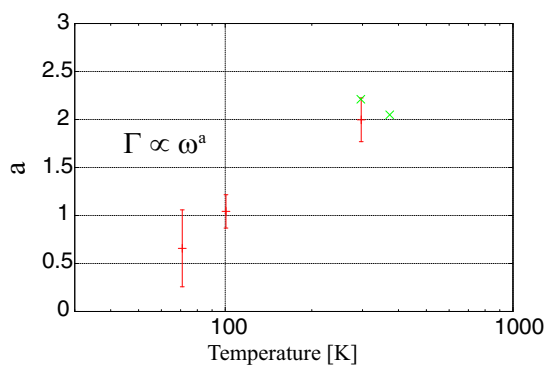


FIG. 8. Frequency dependence of the Brillouin linewidth in the [110] L-mode phonon of TeO₂ as a function of temperature.

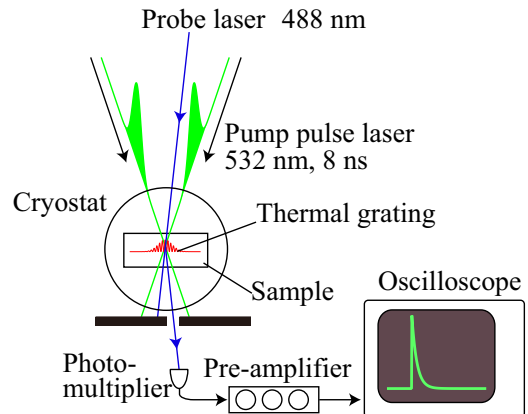


FIG. 9. A schematic of the impulsively stimulated thermal scattering (ISTS) method for measuring thermal phonon lifetimes. The probe laser was scattered by the thermal grating generated by the pump pulses. The scattered probe intensity varying in time was measured with an oscilloscope.

[13,15]. However, the lifetimes of actual thermal phonons are finite. Here we experimentally estimate the lifetime using ISTS measurement. In ISTS measurement, the phonon lifetime is estimated by the duration time of a diffracted light due to the thermal grating impulsively generated by a pulsed laser interference. This method was experimentally developed by Eichler *et al.* [37], and its theoretical treatments were comprehensively discussed by Yan and Nelson [38,39]. We used the same experimental setup with that reported previously [40]. A schematic of the experimental setup for ISTS measurement is shown in Fig. 9. A frequency doubled Nd:YAG laser was used for a pump laser. Its wavelength and pulse width were 532 nm and 8 ns, respectively. For a probe beam, we used a continuous wave Ar ion laser whose wavelength was 488 nm. The pulse beam was split in two paths and focused into a TeO₂ crystal with an intersecting angle of 9.14 mrad in order to make a thermal grating by their interference. Simultaneously, a probe beam was incident to the crystal and the Bragg-diffracted light due to the thermal grating was detected by a photomultiplier. The transient signal of the diffracted light was measured by an oscilloscope after amplification.

The thermal grating decays with the diffusion of the local thermal distribution due to the thermal diffusion process. From this measurement, one can obtain the decay rate of the thermal distribution Γ_{therm} and can derive the thermal diffusion constant D as $D = \Gamma_{\text{therm}}/q^2$, where q is the wave number of the thermal grating [40]. Consequently, the lifetime of thermal phonon τ is given as

$$\tau = 3D/v^2 = \frac{3\Gamma_{\text{therm}}}{q^2v^2}, \quad (9)$$

where v is the sound velocity. It is worth noting that, by ISTS, one can obtain the lifetime of the “resistive” thermal phonons in the hydrodynamic (and diffusive) phonon regime [41]. Thus, unless the normal phonon scattering (N process) is dominant, ISTS gives a reasonable estimate of the thermal phonon lifetimes consistent with those estimated from literature values of the specific heat and the thermal conductivity [40–42]. Since

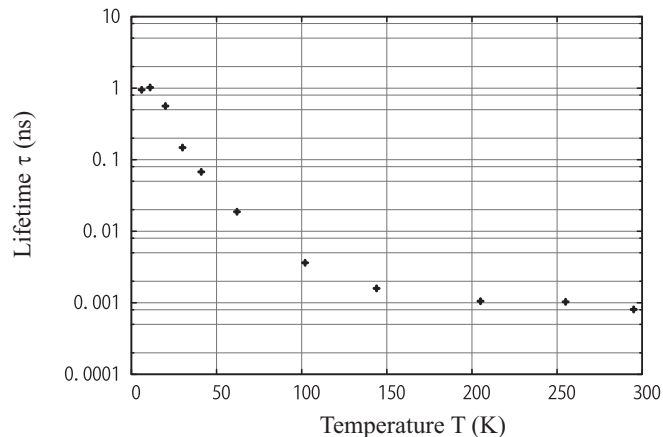


FIG. 10. Temperature dependence of the thermal phonon lifetime estimated by the ISTS measurement.

second sound has not been observed in TeO₂, N process is not considered to be dominant. Therefore, ISTS should give us a reasonable estimate of the thermal phonon lifetime relevant to the attenuation of the longitudinal sound wave investigated here.

Our result of temperature dependence of thermal phonon lifetime is shown in Fig. 10. In this derivation, we used $v = 2.3 \times 10^3$ m/s, which is the mean value of the transverse and longitudinal sound velocities. In our experiment, the value of q was 1.08×10^5 m⁻¹. The lifetime becomes longer as the temperature decreases. Compared with the reported values, the order of our results at 77 and 300 K due to ISTS are in good agreement with the lifetime in TeO₂ reported by Ewbank and Newman [43]. The plateau of the lifetime around 1 ns, shown in the low-temperature region, is caused by the time resolution of the oscilloscope that we used.

IV. DISCUSSION

A. Above Debye temperature

First, we discuss the behavior of the attenuation rate in the relatively high-temperature region. The Debye temperature of TeO₂ has been reported to be around 230 K [7,44]. As shown in Fig. 6, around the Debye temperature, the attenuation linearly depends on temperature. Furthermore, in the temperature region, $T > 300$ K, the temperature dependence b of the attenuation rate in $\Gamma \propto T^b$ decreases with increasing temperature and becomes lower than unity. This behavior is consistent with the attenuation rate, Eq. (4), given by the Akhiezer theory. Around room temperature, which is higher than Debye temperature in TeO₂, the thermal conductivity κ in a phonon gas model can be given as

$$\kappa = \frac{1}{3} C v l, \quad (10)$$

where C and l are the specific heat and mean free path of thermal phonons, respectively [1]. In the Debye model, the specific heat depends little on temperature above the Debye temperature; this is well known as the Dulong-Petit law. The sound velocity v in TeO₂ also depends little on temperature, as shown in the Brillouin shift [7]. The temperature dependence of the mean free path of thermal phonons is given as $l \propto 1/T$ in

the sufficiently high-temperature region [34]. Hence, at higher temperatures, the index b may be lower than unity. On the other hand, we obtained the power of the frequency dependence a is around 2 in this temperature region as shown in Fig. 8. This fact also supports the Akhiezer theory given in Eq. (4). From these results, we can conclude that the hypersonic attenuation process of the L-mode phonon in TeO₂ above the Debye temperature is given by Akhiezer theory.

B. Below Debye temperature

Here we discuss the attenuation rate below the Debye temperature. In this temperature region, it has been believed that the $L + L \rightarrow L$ process, corresponding to $\Gamma \propto \omega^1 T^4$, is forbidden and the Herring process of $L + ST \rightarrow FT$, in which $\Gamma \propto \omega^2 T^3$, is allowed according to Ref. [15]. However, it seems that our experimental results T^4 shown in Fig. 6 support the $L + L \rightarrow L$ process, and the frequency dependence, $a \sim 1$, below 100 K shown in Fig. 8 does not conflict with $\omega^1 T^4$.

1. Comparison with Herring process

According to theoretical predictions [14,15], if $L + L \rightarrow L$ is not dominant, the Herring process should dominate in anisotropic crystals. However, our results for both the temperature and frequency dependences are not consistent with Herring's prediction of $\Gamma \propto \omega^2 T^3$. Firstly, we compare the absolute value of the attenuation rate of our result with the expected value under the Herring process. If our result is larger than the prediction, it implies that a process other than the Herring process is dominant. Otherwise, the Herring process may originally not occur for an unknown reason(s) at least in our experiments.

According to Ref. [15], the attenuation rate is given as

$$\Gamma = A(\theta, \phi) \omega^2 T^3, \quad (11)$$

where the proportional parameter $A(\theta, \phi)$ depends upon the propagation directions θ and ϕ of the phonon, and the value in TeO₂ is given as shown in Table II.

In Fig. 11, the temperature dependence of the attenuation rate obtained using A in the [110] direction and the Brillouin shift, $\omega_B/2\pi = 20.3193$ GHz, at helium temperature [7] is indicated by the blue line with our experimental data of red points and the pink line proportional to T^4 . The unit of the vertical axis is scaled according to the literature. At temperatures above 20 K, in which the measurement accuracy is sufficient, the attenuation rate in our result is similar to, or larger than, that obtained in the Herring process. This fact suggests that the phonon attenuation through an attenuation channel dominates over the Herring process.

Here, we show additional evidence that suggests that attenuation processes other than the Herring one exist. As shown in Table II, the Herring process is forbidden in the [001] direction by symmetry [15]. We also measured the attenuation

TABLE II. Proportional factor $A(\text{sK}^{-3})$ in TeO₂ [15].

| Direction | [001] | [100] | [110] |
|-------------------------|-------|------------------------|------------------------|
| A (sK ⁻³) | 0 | 1.97×10^{-22} | 7.96×10^{-22} |

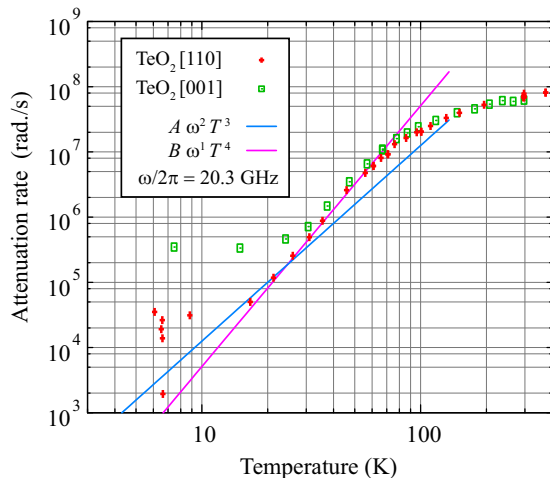


FIG. 11. Comparison of attenuation rates between our results and the Herring process in TeO₂. Attenuation rates measured in [110] and [001] directions are depicted with red and green point, respectively. Since the phonon resonance effect was not observed in the Brillouin spectra measured in the [001] direction, the determination accuracy of attenuation rate was lower than that in the [110] direction at low temperatures. The blue colored line represents $A\omega^2 T^3$ with $A = 7.69 \times 10^{-22} [(\text{rad./s})^{-1}\text{K}^{-3}]$, which is estimated from Eq. (11) for the [110] direction. The pink colored line represents $B\omega^1 T^4$. $B = 4 \times 10^{-12} (\text{K}^{-4})$ is observed in Fig. 6. For both lines, $\omega/2\pi = 20.3193 \text{ GHz}$ is used.

rate in the [001] direction, even though the accurate attenuation rate utilizing the phonon resonance could not be observed because the divergence index of [001] was lower than that of [110]. The estimated attenuation rate is shown with green symbols in Fig. 11. The behavior is very similar to that in the [110] direction between room temperature and 30 K. The attenuation rate below 30 K could not be defined with accuracy because of the transit time broadening of Brillouin spectra. It is noteworthy that the attenuation rate of [001] is similar to, or slightly larger than, that of [110] in which the Herring process is allowed. Furthermore, the temperature dependence goes as T^4 . These suggest that another process exists beside the Herring one. The Brillouin shift in the [001] direction reached 17.928 GHz with decreasing temperature [7].

2. Validity of $L + L \rightarrow L$

In order to identify an attenuation process which depends on T^4 as mentioned above, we come back to the possibility that the $L + L \rightarrow L$ process exists from points of view of the energy- and momentum- conservation within the three-phonon process. As reviewed in the theoretical section, the three-phonon process of $L + L \rightarrow L$ is unlikely to occur for two reasons. The first is the severe condition of satisfying both energy and momentum conservation, as shown in Fig. 3. The second reason is the frequency dispersion of the acoustic phonon in TeO₂. If the dispersion of the acoustic phonon between frequency and wave number is deviated from a linear relation, the momentum cannot be conserved in the scattering process. In this section we re-consider these situations with involving the thermal phonon lifetime.

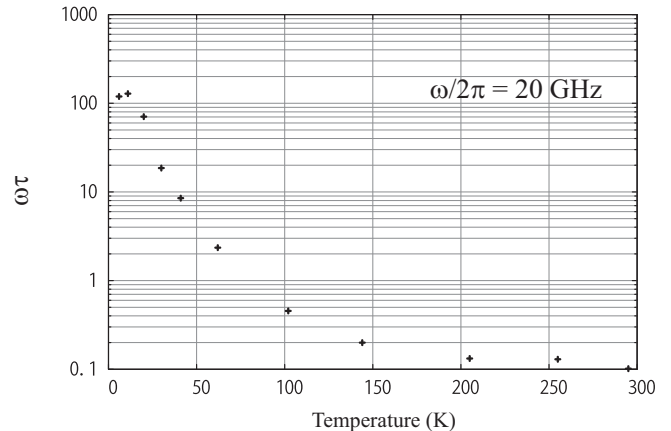


FIG. 12. Temperature dependence of the estimated value of $\omega\tau$ for $\omega/2\pi = 20 \text{ GHz}$.

Because of the uncertainty of the energy under a finite lifetime for the thermal phonon, the energy conservation $\delta(\Delta\omega)$, where $\Delta\omega = \omega_{\Lambda_1} + \omega_{\Lambda_2} - \omega_{\Lambda_3}$ in Eq. (1), should be rewritten as

$$\delta(\Delta\omega) = \lim_{\tau \rightarrow \infty} \frac{\tau}{2\pi\hbar} \frac{\sin^2(\Delta\omega\tau/2)}{(\Delta\omega\tau/2)^2}. \quad (12)$$

This means that the energy has an uncertainty of $2\pi\hbar/\tau$. If this is sufficiently smaller than the phonon energy, it can be ignored. In order to estimate the magnitude, the relationship between the uncertainty and phonon energy $\omega\tau$ is a convenient index. If $\omega\tau$ is sufficiently larger than unity, the energy conservation in the three-phonon process is acceptable. We estimated the temperature dependence of $\omega\tau$ for a phonon with $\omega/2\pi = 20 \text{ GHz}$ using the result from the ISTS measurement, as shown in Fig. 12. This figure indicates that uncertainties of a few percent and several tens of percent are expected around 20 and 50 K, respectively. This means that we have to treat the $\Delta\omega$ as a finite value in this temperature region. Note that $\omega\tau \sim 1$ around 70 K at which the frequency dependence a was around unity as shown in Fig. 8, and below which the temperature dependence met T^4 as shown in Figs. 6 and 11. It seems that the predominant attenuation process gradually changes from the Akiezer regime to the three-phonon scattering regime through this temperature region.

Here, we treat the actual dispersion curve of acoustic phonon mode in TeO₂. Kimura and Sato investigated the phonon modes in TeO₂ and drew their band diagram in Ref. [45]. We traced this diagram in the $[\xi, \xi, 0]$ direction and enlarged it in Fig. 13. In this figure, the vertical axis is converted from energy to temperature using the relation $1 \text{ K} \simeq 0.7 \text{ cm}^{-1}$. The L-mode branch seems to be the third curve drawn from the lowest energy on the Γ point. We found that the dispersion curve of the L-mode phonon behaved almost as linear functions at temperatures below 50 K. This means that the $L + L \rightarrow L$ process is not suppressed by the frequency dispersion of the phonon in the temperature region below 50 K.

Next, using the long-wavelength approximation ($\omega/v = \text{const.}$), we considered the effect of energy uncertainty on the momentum matching in the $L + L \rightarrow L$ process. As shown

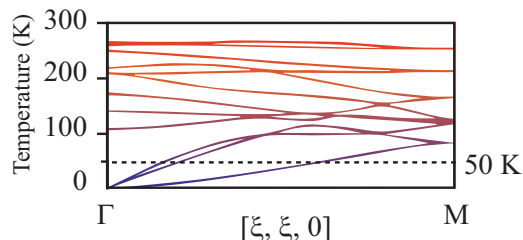


FIG. 13. Phonon dispersion relation in the [110] direction of TeO₂. The data were traced in the low-energy region given by Fig. 3 in Ref. [45]. The vertical axis was reduced from energy to temperature using $1 \text{ K} \simeq 0.7 \text{ cm}^{-1}$.

in Fig. 3, the slowness surfaces touched one another only at a point P . However, if the thermal phonons had finite lifetimes, this condition could be relaxed. We numerically calculated how much uncertainty of energy could be accepted in the relation of $\omega_1 + \omega_2 = \omega_3 + \Delta\omega$ on the slowness surface of ω_2 while keeping \mathbf{q}_1 along the [110] direction. The results are shown in Fig. 14. In this calculation, the ratio between ω_2 and ω_1 was set to $\omega_2/\omega_1 = 20$. Since the energy of $\omega_1 \sim 20 \text{ GHz}$ is nearly equal to 1 K , this condition corresponds to the situation at 20 K . The red area shown in Fig. 14 indicates that $\Delta\omega$ of only 1% permits the relaxed energy conservation rule to be established, and its shape is directly interpreted as a contact area between slowness surfaces of ω_2 and ω_3 . This is not a point contact any longer. We found the scattering area to be very sensitive to decreases of a few percent of $\Delta\omega$ because

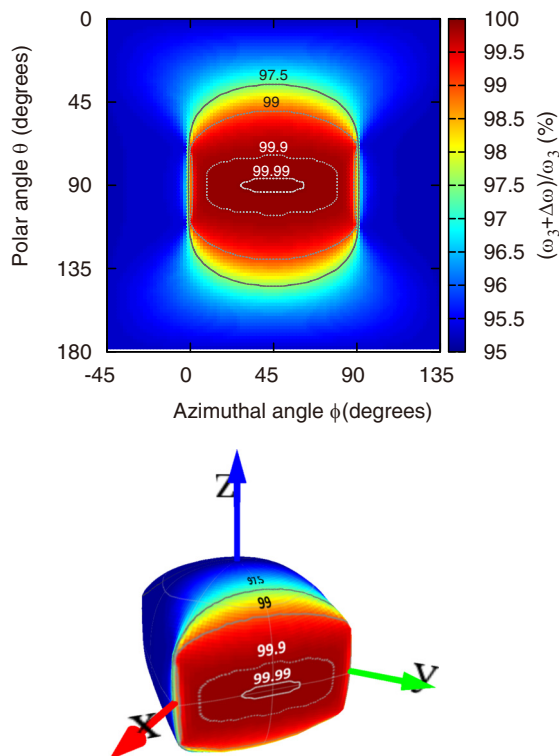


FIG. 14. The area satisfying $\omega_1 + \omega_2 = \omega_3 + \Delta\omega$ with varying $\Delta\omega$ around the [110] direction for the $L + L \rightarrow L$ process in TeO₂. (Upper) mapping in the θ, ϕ plane. (Lower) three-dimensional mapping of the slowness surface of the L-mode phonon.

of the flat shape of the slowness surface around the [110] direction (see the lower panel in Fig. 14). Compared with the phonon lifetime estimated from Fig. 12 around 20 K , it seems that the condition of $\omega_1 + \omega_2 = \omega_3 + \Delta\omega$ is easily satisfied in a finite scattering area on the slowness surface. The similar sensitivities are observed at 5 and 10 K as the scattering area little changed with temperature. Thus, the finite lifetime of the thermal phonon allows attenuation by the $L + L \rightarrow L$ process, explaining the T^4 dependence.

The $L + FT \rightarrow FT$ process, in which the attenuation rate has the same dependence of $\omega^1 T^4$ with the $L + L \rightarrow L$ process, has been discussed with a finite thermal phonon lifetime in prior works in quartz. In the discussion, due to the large mode dispersion, the temperature range to allow this process is quite limited in the vicinity of the situation $\omega\tau \sim 1$ [17]. This situation is similar to our TeO₂ case. As is shown in Fig. 17 in Appendix B, the $L + FT \rightarrow FT$ process requires much larger energy uncertainty to satisfy the relaxed energy conservation rule compared with the $L + L \rightarrow L$ process. We consider the $L + FT \rightarrow FT$ process is also able to occur in a quite narrow temperature range of $\omega\tau \sim 1$, namely $50\text{--}70 \text{ K}$ in TeO₂ though, at least below that temperature range, the $L + L \rightarrow L$ process should be a predominant cause of T^4 dependence. Furthermore, we did not observe the strong temperature dependence (exponent of higher than 4) in the lower temperature unlike the report on quartz. Considering the shape of a slowness surface of L mode along the [110] direction of TeO₂, we suppose this difference comes from the temperature dependence of τ to be attributed to the flatness of slowness surface.

V. CONCLUSION

We investigated the attenuation process of L-mode phonons in TeO₂ by exploiting high-resolution Brillouin scattering and ISTS measurements. We proposed two kinds of indices for the divergence and pure propagation of phonon in an anisotropic crystal. By using these indices, we found the [110] direction in TeO₂ is the most suitable direction for a precise Brillouin measurement. Above the Debye temperature, the attenuation behavior can be understood by considering Akhiezer's damping. In the lower-temperature region, the $L + L \rightarrow L$ process, which depends upon T^4 , exceeds the previously-predicted Herring process. The finite thermal phonon lifetime is a key for the occurrence of the $L + L \rightarrow L$ process. To observe the Herring process in a TeO₂ crystal, one should investigate the lower-temperature region in which the thermal phonon lifetime is sufficiently long.

ACKNOWLEDGMENTS

Authors appreciate Prof. Shin-ichiro Tamura for the fruitful discussion. Authors would like to thank Terumasa Nagano for providing the experimental data and many discussions in the ISTS measurements.

APPENDIX A: PHONON DIVERGENCE AND PURE PROPAGATION

Here, we introduce two indices indicating phonon divergence and pure propagation, respectively. These indices

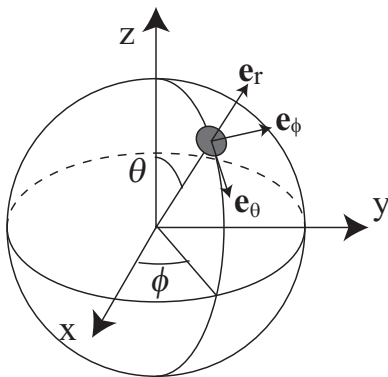


FIG. 15. Polar coordinates in a crystalline direction.

are based on separate viewpoints of phonon propagation in anisotropic crystals. Both conditions contribute to determination of the best direction in a given crystal so as to obtain fine Brillouin spectra at low temperatures.

1. Wave equation

The propagation of a sound wave with wave vector \mathbf{q} and frequency ω can be described by Christoffel's equation:

$$(\rho v^2 \delta_{ik} - C_{ijkl} \hat{q}_j \hat{q}_l) e_k = 0, \quad (\text{A1})$$

where ρ , $v(=\omega/q)$, and C_{ijkl} are, respectively, the density, the sound velocity, and the elastic stiffness tensor of the crystal, e_k is the k th component of a unit vector along a vibrational direction, $\hat{\mathbf{q}} = \mathbf{q}/|\mathbf{q}|$ is a unit vector along the direction of the wave vector, and δ_{ij} is the Kronecker delta. The equation

$$\det |\rho v^2 \delta_{ik} - C_{ijkl} \hat{q}_j \hat{q}_l| = 0 \quad (\text{A2})$$

should be satisfied if nontrivial solutions of Christoffel's equation exist. By solving this eigenvalue problem for the fixed wave vector direction of $\hat{\mathbf{q}}$, one can derive the phase velocity v and the corresponding vibrational eigenmode \mathbf{e} . Generally, this equation gives three independent propagation modes for a certain direction. One is an L mode whose velocity is the fastest. The others are two transverse modes classified by the velocity as FT and ST mode. The sets of phase velocities for all solid angles make surfaces for each mode and are known as the phase-velocity surfaces. In isotropic media, the surface has a spherical shape. In a general crystal, this shape may be deformed due to the anisotropy of the stiffness tensor. As is well known [46], the relation between the group velocity \mathbf{v}_g

given $v_{g_i} = \frac{\partial \omega}{\partial q_i}$ and the energy flux $\langle P_i \rangle$ is given by

$$\langle P_i \rangle = \frac{1}{2} \rho A^2 \omega^2 v_{g_i}, \quad (\text{A3})$$

where A is the amplitude of the sound wave. This means that the direction of the group velocity identifies the direction of the energy flux. The reciprocal of the phase velocity is proportional to the wave number $|\mathbf{q}|$ and is called the slowness. When the frequency ω is fixed, the set of slownesses for all solid angles form a surface, which is known as the slowness surface. On the slowness surface, $\partial \omega(\mathbf{q}) / \partial \mathbf{q} \cdot d\mathbf{q} = \mathbf{v}_g \cdot \mathbf{q} = 0$ is satisfied. Thus, the energy of the sound wave with wave vector \mathbf{q} propagates in a direction normal to the corresponding slowness surface. This significant feature of the sound wave is convenient for estimating the degree of phonon divergence.

2. Definition and derivation

As mentioned above, the propagation direction (energy flux) of a phonon at a certain frequency disperses with the direction of wave vector in a general crystal. In a relatively dispersive direction, the phonon diverges while propagating in the crystal and the effective interaction length between the phonon and light beams in the Brillouin scattering process becomes short. For the same reason, the propagation direction of a phonon is also important. If the propagation direction tilts away from the wave vector, the phonon escapes from the interaction region as it propagates in the medium. Such effects are dominant in measurements at low temperature, where the mean free path of the measured phonon may be longer than the interaction region, rather than at room temperature, where the phonon becomes extinct within a range sufficiently shorter than the interaction region. Here, we propose methodologies for finding the directions in which the divergence of a phonon is minimized and the propagation direction perfectly overlaps with the optical axis, i.e., pure propagation.

In order to estimate the divergence of the phonon, we introduce the index obtained from the following procedure:

(1) Derive the group velocity vector, $\mathbf{v}_g(\theta, \phi)$, for all directions in the polar coordinate shown in Fig. 15 after solving Christoffel's equation.

(2) Derive a vector,

$$\mathbf{v}'_g(\theta, \phi) \equiv \frac{\mathbf{v}_g}{v_{gr}} = \left(1, \frac{v_{g\theta}}{v_{gr}}, \frac{v_{g\phi}}{v_{gr}} \right), \quad (\text{A4})$$

whose component in the \mathbf{e}_r direction, i.e., the direction of \mathbf{q} , is unity.

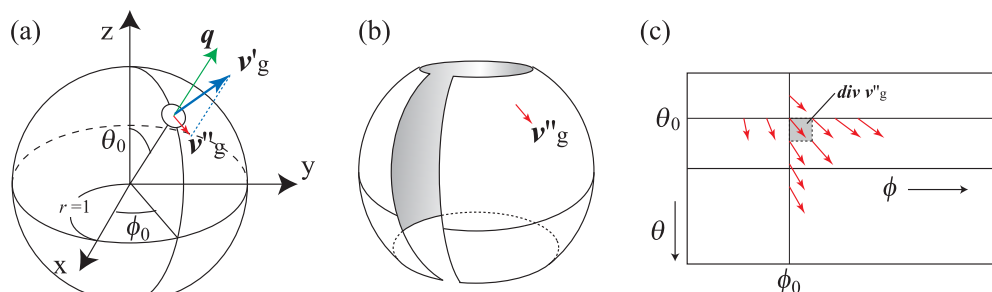


FIG. 16. Schematics of the proposed index for divergence. (a),(b) Projection of the normalized group velocity onto a sphere of $r = 1$. (c) The divergence of the normalized group velocity in a (θ, ϕ) plane.

(3) Project \mathbf{v}'_g onto a sphere with unit radius [Figs. 16(a) and 16(b)] as

$$\mathbf{v}''_g(\theta, \phi) \equiv \begin{pmatrix} v_{g\theta} & v_{g\phi} \\ v_{gr} & v_{gr} \end{pmatrix}, \quad (\text{A5})$$

which is defined on a two-dimensional (θ, ϕ) plane.

(4) Calculate the in-plane divergence as

$$\text{div}_{\theta, \phi} \mathbf{v}''_g(\theta, \phi), \quad (\text{A6})$$

which is an index of the phonon divergence [Fig. 16(c)].

This index indicates the degree of divergence of the phonon in a crystalline direction. For example, in the direction in which the value of the index is large, the phonon beam should diverge while propagating. One should determine the direction in which the value becomes minimal. If the group velocity vector is normal to the sphere of $r = 1$, the length of \mathbf{v}''_g on the (θ, ϕ) plane and the index of divergence should be zero. Hence, in the isotropic material whose slowness surface is spherical in shape, the index of the divergence should be zero all around. In the direction where the index is much smaller than zero, the phonon may be defocused after experiencing tight focusing. However, such a situation cannot occur for the L-mode phonon, because its slowness surface cannot have negative curvature [28]. Around the smallest index direction on the L-mode slowness surface, the group velocity vectors will be likely parallel, rather than crossing. Note that to simplify the calculation for the L-mode phonon, we introduced the index shown above; however, for precise treatment of the divergences including FT- or ST-mode phonons, whose slowness surfaces can have negative curvatures, the Gauss curvature of the slowness surface may be convenient.

Next, we introduce another index for the pure-propagation direction in which the direction of energy flux tends to be the same as that of the wave vector. If the angle between these directions is finite, the concerning sound wave in the Brillouin scattering process deviates from the interaction region with propagation. Here, we adopt the angle β between the direction of the energy flux and the wave vector as an index for pure propagation. The index of purity can be obtained as

$$\beta = \arccos \left(\hat{\mathbf{q}} \cdot \frac{\mathbf{v}_g}{|\mathbf{v}_g|} \right). \quad (\text{A7})$$

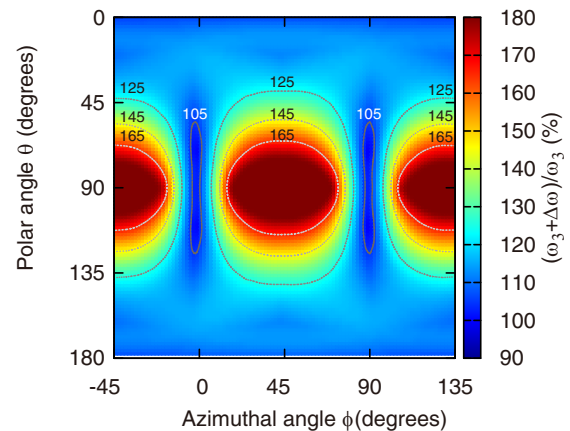


FIG. 17. The area satisfying $\omega_1 + \omega_2 = \omega_3 + \Delta\omega$ with varying $\Delta\omega$ around the [110] direction for the $L + FT \rightarrow FT$ process in TeO_2 .

One can obtain the pure propagation direction as a result of the numerical calculation of the distribution of β in the (θ, ϕ) plane.

APPENDIX B: POSSIBILITY OF $L + FT \rightarrow FT$

Here, assuming the long-wavelength approximation ($\omega/v = \text{const.}$), we considered the effect of energy uncertainty on the momentum matching in the $L + FT \rightarrow FT$ process as well as the $L + L \rightarrow L$ process shown in Fig. 14. The calculation was performed under the same condition with Fig. 14 except for the oscillation mode of the thermal phonons. A slowness surface for an FT mode is larger than that for an L mode and has both positive and negative curvature [29]. The result is shown in Fig. 17. This figure shows that the energy uncertainty $\Delta\omega$ itself should become comparable with ω_3 in order to satisfy the condition of $L + FT \rightarrow FT$ in the sufficiently wide area on the map, whereas the only few percent of uncertainty is necessary in the $L + L \rightarrow L$ process. Hence, $L + FT \rightarrow FT$ could be allowed under the condition of $\tau \sim 1/\omega$ which is quite limited comparing with the $L + L \rightarrow L$ process. Therefore we consider $L + L \rightarrow L$ process is dominant in the temperature range of $\omega\tau > 1$, i.e., $T < 50$ K.

- [1] C. Kittel, *Introduction to Solid State Physics*, 7th ed. (Wiley, New York, 1995).
 [2] H. Maris, ed., *Phonon Scattering in Condensed Matter* (Plenum Press, New York, 1980).
 [3] Y. S. Ju and K. E. Goodson, *Appl. Phys. Lett.* **74**, 3005 (1999).
 [4] R. Anufriev, J. Maire, and M. Nomura, *Phys. Rev. B* **93**, 045411 (2016).
 [5] S. Ohno, T. Sonehara, E. Tatsu, A. Koreeda, and S. Saikan, *Rev. Sci. Instrum.* **77**, 123104 (2006).
 [6] T. Sonehara, Y. Konno, H. Kaminaga, S. Saikan, and S. Ohno, *J. Opt. Soc. Am. B* **24**, 1193 (2007).

- [7] T. Sonehara, E. Tatsu, S. Saikan, and S. Ohno, *J. Appl. Phys.* **101**, 103507 (2007).
 [8] T. Sonehara, Y. Konno, H. Kaminaga, and S. Saikan, *J. Korean Phys. Soc.* **51**, 836 (2007).
 [9] T. Sonehara, H. Kaminaga, E. Tatsu, S. Saikan, and S. Ohno, *J. Non-Cryst. Solids* **354**, 1768 (2008).
 [10] T. Sonehara, H. Kaminaga, E. Tatsu, S. Saikan, and S. Ohno, *Opt. Lett.* **32**, 808 (2007).
 [11] T. Sonehara, H. Kaminaga, E. Tatsu, S. Saikan, and S. Ohno, *J. Appl. Phys.* **101**, 073104 (2007).
 [12] S. Ohno, T. Sonehara, E. Tatsu, A. Koreeda, and S. Saikan, *Phys. Rev. B* **92**, 214105 (2015).

- [13] E. P. N. Damen, A. F. M. Arts, and H. W. de Wijn, *Phys. Rev. B* **59**, 349 (1999).
- [14] C. Herring, *Phys. Rev.* **95**, 954 (1954).
- [15] S. Tamura, A. Sangu, and H. J. Maris, *Phys. Rev. B* **68**, 014302 (2003).
- [16] M. F. Lewis and E. Patterson, *Phys. Rev.* **159**, 703 (1967).
- [17] G. P. Barton and W. G. B. Britton, *Acta Acustica united with Acustica* **41**, 207 (1978).
- [18] R. Nava and M. Rodriguez, *Phys. Rev. B* **4**, 4512 (1971).
- [19] Yu. V. Ilisavskii and V. M. Sternin, *Sov. Phys. Solid State* **27**, 236 (1985).
- [20] T.-M. Liu, S.-Z. Sun, C.-F. Chang, C.-C. Pan, G.-T. Chen, J.-I. Chyi, V. Gusev, and C.-K. Sun, *Appl. Phys. Lett.* **90**, 041902 (2007).
- [21] R. Legrand, A. Huynh, B. Jusserand, B. Perrin, and A. Lemaître, *Phys. Rev. B* **93**, 184304 (2016).
- [22] P. Nagpal, N. C. Lindquist, S.-H. Oh, and D. J. Norris, *Science* **325**, 594 (2009).
- [23] V. G. Kravets, S. Neubeck, A. N. Grigorenko, and A. F. Kravets, *Phys. Rev. B* **81**, 165401 (2010).
- [24] M. J. P. Musgrave, *Crystal Acoustics* (Holden-day, San Francisco, 1970).
- [25] G. P. Srivastava, *The Physics of Phonons* (Adam Hilger, Bristol, England, 1990).
- [26] H. J. Maris, *Physical Acoustics* **8**, 279 (1971).
- [27] H. J. Maris, *J. Acoust. Soc. Am.* **50**, 812 (1971).
- [28] J. P. Wolfe, *Imaging Phonons: Acoustic Wave Propagation in Solids* (Cambridge University Press, New York, 2005).
- [29] D. C. Hurley, J. P. Wolfe, and K. A. McCarthy, *Phys. Rev. B* **33**, 4189 (1986).
- [30] L. Landau and G. Rumer, *Phys. Z. Sowjetunion* **11**, 18 (1937).
- [31] R. W. Boyd, *Nonlinear Optics* (Academic Press, San Diego, 1992).
- [32] A. Akhiezer, *J. Phys. (USSR)* **1**, 277 (1939).
- [33] T. O. Woodruff and H. Ehrenreich, *Phys. Rev.* **123**, 1553 (1961).
- [34] J. M. Ziman, *Principles of the Theory of Solids* (Cambridge University Press, New York, 1969).
- [35] R. Vacher and E. Courtens, *International Tables for Crystallography*, Vol. D: Physical properties of crystals (International Union of Crystallography, 2006), Chap. 2.4, p. 335.
- [36] S. Singh, W. A. Bonner, and L. G. V. Uitert, *Phys. Lett. A* **38**, 407 (1972).
- [37] H. Eichler, G. Salje, and H. Stahl, *J. Appl. Phys.* **44**, 5383 (1973).
- [38] Y.-X. Yan and K. A. Nelson, *J. Chem. Phys.* **87**, 6240 (1987).
- [39] Y.-X. Yan and K. A. Nelson, *J. Chem. Phys.* **87**, 6257 (1987).
- [40] A. Koreeda, T. Nagano, S. Ohno, and S. Saikan, *Phys. Rev. B* **73**, 024303 (2006).
- [41] A. Koreeda, R. Takano, and S. Saikan, *Phys. Rev. B* **80**, 165104 (2009).
- [42] A. Koreeda, R. Takano, A. Ushio, and S. Saikan, *Phys. Rev. B* **82**, 125103 (2010).
- [43] M. D. Ewbank and P. R. Newman, *Solid State Commun.* **39**, 303 (1981).
- [44] M. Barucci, C. Brofferio, A. Giuliani, E. Gottardi, I. Peroni, and G. Ventura, *J. Low Temp. Phys.* **123**, 303 (2001).
- [45] N. Kimura and T. Sato, *J. Phys. Soc. Jpn.* **63**, 3704 (1994).
- [46] D. Royer and E. Dieulesaint, *Elastic Waves in Solids I Free and Guided Propagation* (Springer-Verlag, Berlin, Heidelberg, 1999).